Journal of Power Sources 242 (2013) 589–596

Contents lists available at SciVerse ScienceDirect

Journal of Power Sources

journal homepage: www.elsevier.com/locate/jpowsour

Layered $Li[Ni_{0.5}Co_{0.2}Mn_{0.3}]O_2$–$Li_2MnO_3$ core–shell structured cathode material with excellent stability

Xiukang Yang, Xianyou Wang*, Liang Hu, Guishan Zou, Shaojuan Su, Yansong Bai, Hongbo Shu, Qiliang Wei, Benan Hu, Long Ge, Di Wang, Li Liu

Key Laboratory of Environmentally Friendly Chemistry and Applications of Ministry of Education, School of Chemistry, Xiangtan University, Hunan, Xiangtan 411105, China

HIGHLIGHTS

- A $LiNi_{0.5}Co_{0.2}Mn_{0.3}O_2$–$Li_2MnO_3$ core–shell composite was successfully prepared.
- The composite was composed of $LiNi_{0.5}Co_{0.2}Mn_{0.3}O_2$ core and Li_2MnO_3 outer shell.
- The composite showed superior cycling performance and improved thermal stability.
- The improved performance was ascribed to the stability of Li_2MnO_3 outer shell.

ARTICLE INFO

Article history:
Received 5 February 2013
Received in revised form
22 May 2013
Accepted 26 May 2013
Available online 6 June 2013

Keywords:
Lithium ion batteries
Cathode material
Core–shell composite
Layered nickel-rich oxides
Excellent stability

ABSTRACT

In order to improve the performance of the $Li[Ni_{0.5}Co_{0.2}Mn_{0.3}]O_2$, a novel spherical $Li[Ni_{0.5}Co_{0.2}Mn_{0.3}]O_2$–$Li_2MnO_3$ core–shell composite has been successfully synthesized by a simple sol–gel deposition method. It is found that the core–shell composite consists of $Li[Ni_{0.5}Co_{0.2}Mn_{0.3}]O_2$ as the core and Li_2MnO_3 as the outer shell according to examination by scanning electron microscope (SEM) with energy dispersive X-ray spectroscopy (EDXS) and X-ray diffraction (XRD). The core–shell composite delivers a high capacity of 180.4 mAh g^{-1} at a rate of 0.1 C in the voltage range of 2.0–4.4 V. Most importantly, the core–shell composite exhibits excellent capacity retention of 98.8% after 200 cycles at a rate of 0.5 C, and 93.8% capacity retention after 100 cycles at a rate of 5 C at room temperature. When cycled at an elevated 55 °C, the prepared sample exhibits only 2.3% capacity loss after 100 cycles. Meanwhile, the core–shell composite shows significantly improved thermal stability relative to that of the pristine $Li[Ni_{0.5}Co_{0.2}Mn_{0.3}]O_2$. The improved stability of the core–shell composite is ascribed to the stable Li_2MnO_3 outer shell, which can prevent the $Li[Ni_{0.5}Co_{0.2}Mn_{0.3}]O_2$ core from direct contact with the electrolyte, and the core material could operate with no risk of structural disruption at high voltages and high temperatures.

1. Introduction

Rapidly growing demands for energy storage devices, portable electronic devices and electric vehicles will require high performance rechargeable batteries. Among the various rechargeable batteries, the lithium ion batteries have been most intensively used for their outstanding energy and power density performance [1–3]. Although lithium-ion batteries have been widely used in a variety of applications, many issues are still being intensively studied for further improvement. In particular, the development of cathode materials with high energy density and improved stability is one of the hottest topics in lithium ion batteries [4,5].

The key strategy to increase the energy density of battery is to develop cathode materials with higher capacity or higher operating voltages [3,6]. In this regard, very appealing candidate is layered nickel-rich oxide $LiNi_{0.5}Co_{0.2}Mn_{0.3}O_2$ owing to its higher specific capacity, relatively low cost, and less toxicity than $LiCoO_2$, which is the mainstream commercial cathode material nowadays [7–9]. Unfortunately, the wide practical use of the $LiNi_{0.5}Co_{0.2}Mn_{0.3}O_2$ electrode has so far been hindered by its poor cycling performance and inferior thermal stability, especially at high operate voltages (>4.3 V) or high temperatures (>40 °C). The main reason is that the unstable Co^{4+} and Ni^{4+} ions are easily reduced when they contact directly with the electrolyte, increasing the interfacial impedance

* Corresponding author. Tel.: +86 731 58292060; fax: +86 731 58292061.
E-mail address: wxianyou@yahoo.com (X. Wang).

0378-7753/$ – see front matter © 2013 Elsevier B.V. All rights reserved.
http://dx.doi.org/10.1016/j.jpowsour.2013.05.139

and thus decreasing the cycle life of the cells [10]. Concurrently, the delithiated $Li_{1-\delta}[Ni_{0.5}Co_{0.2}Mn_{0.3}]O_2$ material is structurally unstable during thermal runaway reactions due to the oxygen release from the host structure, which can then react with the organic electrolyte causing flame and obvious safety problems [11]. Therefore, even though the layered nickel-rich $LiNi_{0.5}Co_{0.2}Mn_{0.3}O_2$ cathode material has much higher specific capacity, it has been severely restricted by its intrinsic insufficient cycle life and poor thermal stability [9–12].

The surface coating has been proved to be an effective method to improve the electrochemical performance of cathode materials. Various metallic compounds, such as TiO_2, AlF_3 and $FePO_4$, have been reported to be coating materials for improving the cycling performance and thermal stability of $LiNi_{0.5}Co_{0.2}Mn_{0.3}$ cathode material [13–15]. The improvement of the cathode properties upon applying a metallic compound coating is attributed mainly to the improved interface stability between the active material and electrolyte. The inert coating layer can restrict the direct contact between the active material and the electrolyte, so the host structure was protected against HF attack in the electrolyte. Nevertheless, the thin coating layer (<10 nm) is liable to flake off the cathode surfaces during the long-term cycling. Inevitably, the exposed area can be subjected to continuous HF attack, which, eventually, would have a negative effect on its electrochemical and thermal performance [16].

Recently, an effective approach was adopted at Argonne National Laboratory to stabilize layered $LiMO_2$ (M = metal) cathode materials by integrating a structurally compatible component Li_2MnO_3 [17,18]. This type of material is considered as lithium-rich oxides $xLi_2MnO_3\cdot(1-x)LiMO_2$ (M = metal, $x>0$), which is also regarded as a nano-dimensional solid solution between layered $LiMO_2$ and Li_2MnO_3 [18–21]. In this material, the Li_2MnO_3 component is very important because it can lend structural stability and provide additional high capacity to electrode if electrochemically activated above 4.5 V [18]. However, the lithium-rich oxides are still far from real applications because of a number of unsolved issues, such as the huge irreversible capacity loss in the first cycle, which is attributed to the part extraction of the lithium as "Li_2O" followed by an elimination of the oxide ion vacancies from the lattice during the first charge resulting in a lower number of sites for insertion/extraction of lithium ions in the subsequent cycles [22,23], and structural evolution upon insertion–reinsertion of lithium leading to decrease in the discharge plateau with increase of the cycle number [24,25]. Furthermore, the lithium-rich oxides must be charged to considerably high potentials of above 4.6 V to obtain high capacity, which are beyond the electrochemical stable windows (<4.5 V) of the normal electrolytes which are widely used nowadays. However, it is worth mentioning that the Li_2MnO_3 compound is electrochemically inactive when the voltage is less than 4.5 V, because all the manganese ions are tetravalent and cannot be oxidized further. Moreover, lithium insertion into Li_2MnO_3, with a concomitant reduction of the manganese ions, is also prohibited because there are no energetically favorable interstitial sites for the guest ions. Under such conditions, the Li_2MnO_3 compound can act as a stabilizing unit in the electrode structure [26].

Based on the above analysis and consideration, in this work, a new strategy to stabilize the layered nickel-rich $Li[Ni_{0.5}Co_{0.2}Mn_{0.3}]O_2$ is put forward through encapsulation with a stable Li_2MnO_3 outer shell. A spherical $Li[Ni_{0.5}Co_{0.2}Mn_{0.3}]O_2$–$Li_2MnO_3$ core–shell composite was synthesized by a simple sol–gel deposition method. The Li_2MnO_3 compound, which is electrochemical inactive below 4.5 V, was tightly wrapped on the surface of the active $Li[Ni_{0.5}Co_{0.2}Mn_{0.3}]O_2$ core to protect the core from direct attacking by the electrolyte. We expect that, the core–shell composite has the $Li[Ni_{0.5}Co_{0.2}Mn_{0.3}]O_2$ core to deliver high capacity, and a shell made of electrochemical inert Li_2MnO_3 provides excellent cycling life as well as improved thermal stability, especially at high operate voltages and high temperatures.

2. Experimental

2.1. Synthesis of $[Ni_{0.5}Co_{0.2}Mn_{0.3}](OH)_2$ precursor

The $[Ni_{0.5}Co_{0.2}Mn_{0.3}](OH)_2$ precursor was synthesized by a co-precipitation method [27,28]. A mixed solution of $NiSO_4\cdot6H_2O$,

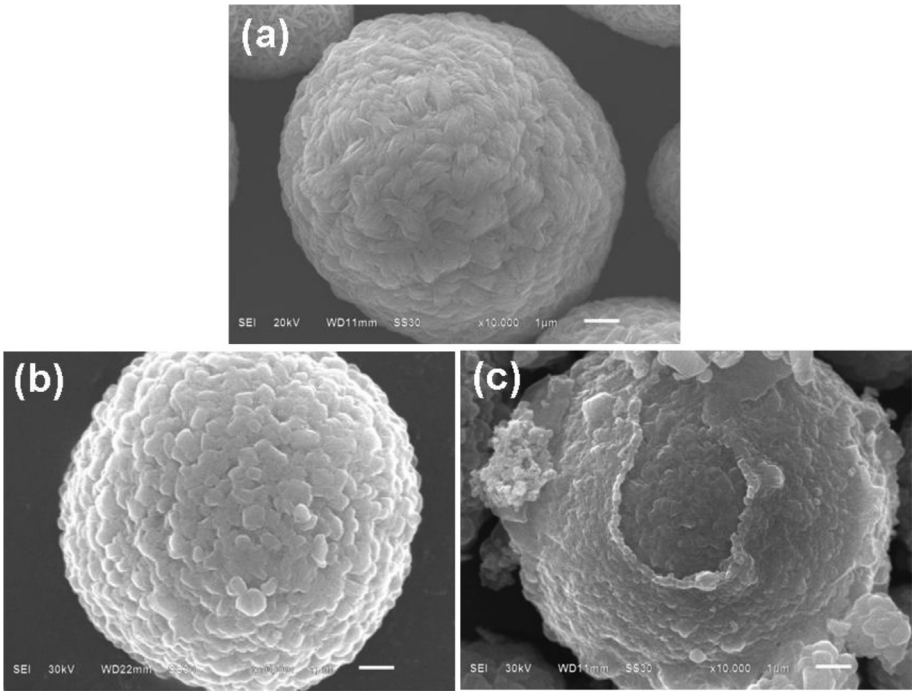

Fig. 1. SEM images of (a) $[Ni_{0.5}Co_{0.2}Mn_{0.3}](OH)_2$ precursor, (b) pristine $Li[Ni_{0.5}Co_{0.2}Mn_{0.3}]O_2$ and (c) $Li[Ni_{0.5}Co_{0.2}Mn_{0.3}]O_2$–$Li_2MnO_3$ core–shell composite particle.

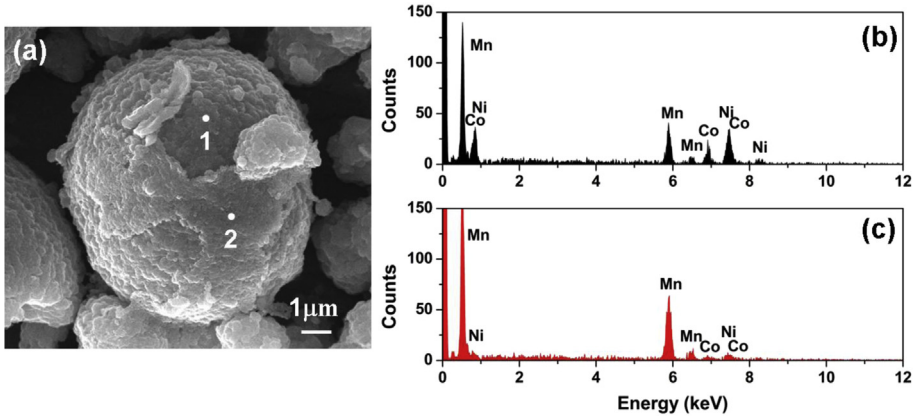

Fig. 2. SEM image and the corresponding EDXS spectrums for the $Li[Ni_{0.5}Co_{0.2}Mn_{0.3}]O_2$–$Li_2MnO_3$ core–shell composite. EDXS was performed at the solid point 1 on the core and point 2 on the shell of the particle to determine the relative Ni, Co and Mn compositions.

$CoSO_4 \cdot 7H_2O$ and $MnSO_4 \cdot H_2O$ (cationic ratio of Ni:Co:Mn = 5:2:3) with total metal ion concentration of 1.6 mol L^{-1}, which was used as the starting materials for the $[Ni_{0.5}Co_{0.2}Mn_{0.3}](OH)_2$ precursor, was pumped into a continuously stirred tank reactor. At the same time, a 3.2 mol L^{-1} NaOH solution (aq) as precipitant and the desired amount of NH_4OH solution (aq) as chelating agent were also separately fed into the reactor. The concentration of the solution, pH (11.00), the operation temperature (55 °C) and the stirring speed (1000 rpm) in the reactor were carefully controlled. The obtained $[Ni_{0.5}Co_{0.2}Mn_{0.3}](OH)_2$ precursor was then filtered, washed, and dried at 110 °C for 12 h.

2.2. Synthesis of $Li[Ni_{0.5}Co_{0.2}Mn_{0.3}]O_2$

The produced $[Ni_{0.5}Co_{0.2}Mn_{0.3}](OH)_2$ precursor was mixed thoroughly with 4% excess lithium hydroxide (excess amount of Li salt was used to compensate for possible Li loss during the calcinations). The mixture was first heated at 500 °C for 6 h in air, then calcined at 850 °C for 12 h in air to obtain $Li[Ni_{0.5}Co_{0.2}Mn_{0.3}]O_2$ powders.

2.3. Synthesis of $Li[Ni_{0.5}Co_{0.2}Mn_{0.3}]O_2$–$Li_2MnO_3$ core–shell composite

To prepare the core–shell composite, a simple sol–gel deposition method was adopted here. An appropriate amount of $[Mn(CH_2COO)_2 \cdot 6H_2O]$ and $LiOH \cdot H_2O$ were dissolved in 100 mL distilled water. The resulting mixed solution was added drop by drop into the continuously agitated aqueous solution of citric acid, which is as a chelating agent. The pH of obtained solution was adjusted in range of 6.0–6.5 by using ammonium hydroxide. Under the effect of the chelating agent, the aqueous solution of manganese acetate and lithium hydroxide was then evaporated at 80 °C under stirring to form a gel. Afterward, the $Li[Ni_{0.5}Co_{0.2}Mn_{0.3}]O_2$ powders were added into the gel and stirred overnight. Finally, the mixture was calcined at 850 °C for 10 h under air to obtain the core–shell composite.

2.4. Materials characterization

The phase identification of the samples was performed with a diffractometer (D/Max-3C, Rigaku) using Cu Kα radiation (λ = 1.54178 Å) and a graphite monochromator at 40 kV, 100 mA. The scanning rate was 8° min^{-1} and the scanning range of diffraction angle (2θ) was $10° \leq 2\theta \leq 80°$. The morphology of the samples was observed using a scanning electron microscopy (SEM). The local composition of the core–shell composite was obtained with an energy-dispersive X-ray spectroscope (EDXS) (JSM-6610LV, JEOL). The chemical compositions of the resulting powders were analyzed by atomic absorption spectroscopy (AAS, Vario 6 Analytik Jena AG, Jena).

2.5. Electrochemical test

In order to fabricate the positive electrode, the as-prepared materials were mixed with acetylene black, graphite and polyvinylidene fluoride (80:5:5:10) in *N*-methyl-2-pyrrolidone. The obtained slurry was coated onto Al foil. The electrodes were dried overnight at 110 °C in a vacuum. Preliminary cell tests were done with a 2025 coin-type cell using Li metal as the anode. The electrolyte solution was a 1 M $LiPF_6$ in ethylene carbonate (EC)–dimethyl carbonate (DMC) (1:1, v/v). Charge–discharge measurement was carried out in neware battery test system BTS-XWJ-6.44S-00052 (Newell, China). The cyclic voltammetry (CV) experiments were carried out at a scan rate of 0.1 mV s^{-1} in the voltage range of 2.0–4.5 V using PARSTAT 2273 electrochemical workstation.

2.6. Thermal properties

For the differential scanning calorimetry (DSC) experiments, the cell were charged to 4.4 V at a current density of 20 mA g^{-1} and disassembled in an Ar-filled dry box. After the remaining electrolyte was carefully removed from the surface of the electrode, the cathode materials were recovered from the current collector. Measurements were carried out in a DSC 200 PC using a temperature scan rate of 5 °C min^{-1}.

3. Results and discussion

In order to determine the chemical composition of the as-prepared materials, AAS analysis was carried out. The chemical composition of hydroxide precursor was $[Ni_{0.502}Co_{0.198}Mn_{0.300}](OH)_2$, which was corresponding to the desired $[Ni_{0.5}Co_{0.2}Mn_{0.3}](OH)_2$. The morphology

Table 1
EDXS data of the $Li[Ni_{0.5}Co_{0.2}Mn_{0.3}]O_2$–$Li_2MnO_3$ core–shell composite.

Element	Point 1 (core)			Point 2 (shell)		
	Ni	Co	Mn	Ni	Co	Mn
At.(%)	48.35	19.08	32.57	2.04	1.24	96.72

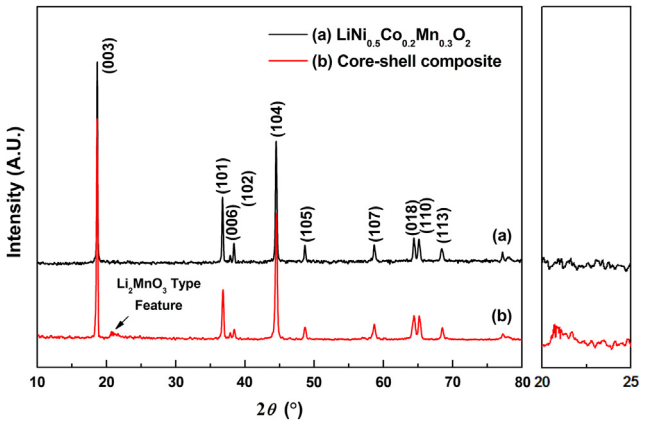

Fig. 3. X-ray diffraction patterns of (a) the pristine $LiNi_{0.5}Co_{0.2}Mn_{0.3}O_2$ and (b) $Li[Ni_{0.5}Co_{0.2}Mn_{0.3}]O_2$–$Li_2MnO_3$ core–shell composite.

of the $[Ni_{0.5}Co_{0.2}Mn_{0.3}](OH)_2$ precursor was examined by SEM, as shown in Fig. 1a. It was a spherical morphology, and the particle size was approximately 9 μm in diameter. In addition, a closer inspection of Fig. 1a clearly indicated that the spherical particle of the $[Ni_{0.5}Co_{0.2}Mn_{0.3}](OH)_2$ precursor was made up of numerous laminated flake primary grains. After the precursor was mixed with $LiOH{\cdot}H_2O$ and calcinated at high temperature, the spherical morphology and particle size of the precursor were maintained. However, the primary particle of the obtained $Li[Ni_{0.5}Co_{0.2}Mn_{0.3}]O_2$ was changed to granular shape, as shown by the SEM image in Fig. 1b. Usually, co-precipitation process is used to prepare the spherical particle, and the analogous works have also been reported elsewhere [27,29].

Fig. 1c shows the SEM image of the $Li[Ni_{0.5}Co_{0.2}Mn_{0.3}]O_2$–$Li_2MnO_3$ core–shell composite. The SEM image clearly indicated the existence of core–shell structure. The core–shell composite had slightly larger particle size than $Li[Ni_{0.5}Co_{0.2}Mn_{0.3}]O_2$ because the shell covered the surface of pristine $Li[Ni_{0.5}Co_{0.2}Mn_{0.3}]O_2$, as anticipated. The thickness of the outer shell was about 0.2–0.3 μm, which was thicker than the previous coatings mentioned in the Introduction section. The core material was firmly enclosed by an outer layer, which could prevent the unstable core from directly contacting with the electrolytes when it is used in the lithium ion battery. Thus, it can be confirmed from the SEM images that the formation of the core–shell structure morphology is successful. The total average chemical composition of core–shell composite was $Li_{1.155}[Ni_{0.422}Co_{0.165}Mn_{0.413}]O_2$ by AAS analysis, indicating that the molar ratio of the core and shell was about 0.85:0.15.

Elemental point analysis using EDXS in SEM is carried out to further determine the local composition in the core and shell material. Fig. 2a shows the SEM image of the core–shell composite particles, which were partially crushed in an agate mortar. The core and shell of the composite were obviously observed in Fig. 2a. The EDXS spectra measured at the positions of the core and shell which were marked as solid points in Fig. 2a are shown in Fig. 2b and c, respectively. The EDXS analytical data are shown in Table 1. From

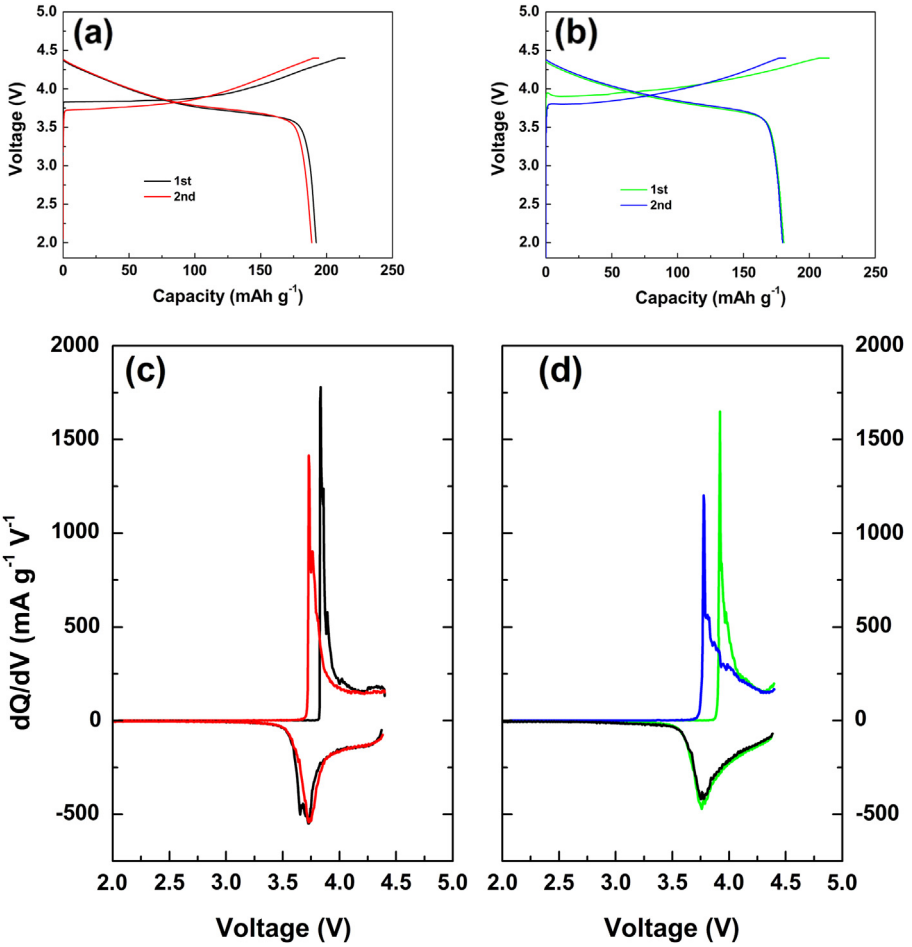

Fig. 4. First and second charge–discharge curves of (a) $Li/Li[Ni_{0.5}Co_{0.2}Mn_{0.3}]O_2$ and (b) Li/core–shell composite cells cycled at a rate of 0.1 C in the voltage range of 2.0–4.4 V; (c) and (d) the corresponding differential capacity profiles of (a) and (b), respectively.

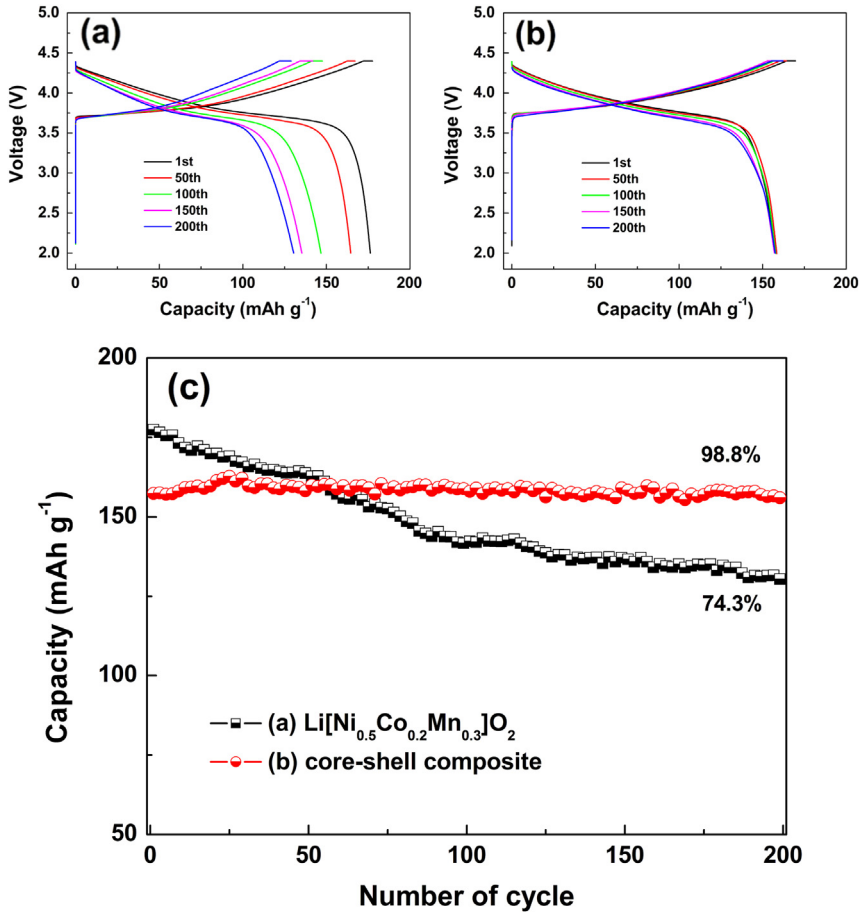

Fig. 5. Continuous charge and discharge curves of (a) $Li[Ni_{0.5}Co_{0.2}Mn_{0.3}]O_2$, (b) core–shell composite cells, and (c) discharge capacity *versus* cycle number of Li/(a), (b) cells at a rate of 0.5 C in the voltage range of 2.0–4.4 V at room temperature.

the EDXS data on point 1 at the surface of the core material, the core was composed of a molar ratio of 0.484 Ni, 0.191 Co and 0.326 Mn, which was close to the ideal core composition of 0.5 Ni, 0.2 Co and 0.3 Mn. The outer layer contained mainly Mn element from the EDXS analysis on the point 2 at the surface of the outer shell, excepting for trace amounts of Ni and Co elements. Calculated from the EDXS spectrum, the molar ratio of Ni:Co:Mn in the coating layer was 0.020:0.012:0.967. The outer layer contained a small amount of Ni and Co, which may due to the element diffusion from the shell to the core and/or the core to the shell during the high temperature calcinations [11,30]. From the EDXS analysis, the local composition of the core and shell of the prepared sample is basically consistent with the desired composition.

The XRD patterns of the pristine $Li[Ni_{0.5}Co_{0.2}Mn_{0.3}]O_2$ and the $Li[Ni_{0.5}Co_{0.2}Mn_{0.3}]O_2$–$Li_2MnO_3$ core–shell composite are shown in Fig. 3. Both the samples exhibited a well-defined layer structure based on a hexagonal α-$NaFeO_2$ structure with a space group of $R\bar{3}m$[29,31]. No differences were observed between the pristine and core–shell material besides some weak diffraction peaks between 20 and 25° for the core–shell composite, indicating a layered structure with Li_2MnO_3 character (space group $C2/m$) [18,20,32–34]. In the idealized Li_2MnO_3 structure, six MnO_6 octahedra surround every LiO_6 octahedron, giving rise to a hexagonal $LiMn_6$ nearest-neighbor unit in the manganese-rich plane that, together with the nearest-neighbor lithium ions in adjacent layers, represents the building block of Li_2MnO_3 [26,35]. However, for the $Li[Ni_{0.5}Co_{0.2}Mn_{0.3}]O_2$ core, it is more difficult to cluster the lithium distinctly around the manganese ions to generate short-range order in the $LiMn_{6-x}M_x$ (M = Ni, Co) hexagonal units because of significantly less manganese content in the core material (from the above EDXS analysis), restricting the growth of the Li_2MnO_3 regions in the transition metal layers [26,36,37]. Consequently, it is most likely that the Li_2MnO_3 structure only exists in the outer layer. Based on the above analysis, it can be verified that the core–shell composite, in which the $Li[Ni_{0.5}Co_{0.2}Mn_{0.3}]O_2$ core was encapsulated with a Li_2MnO_3 outer shell, was successfully synthesized.

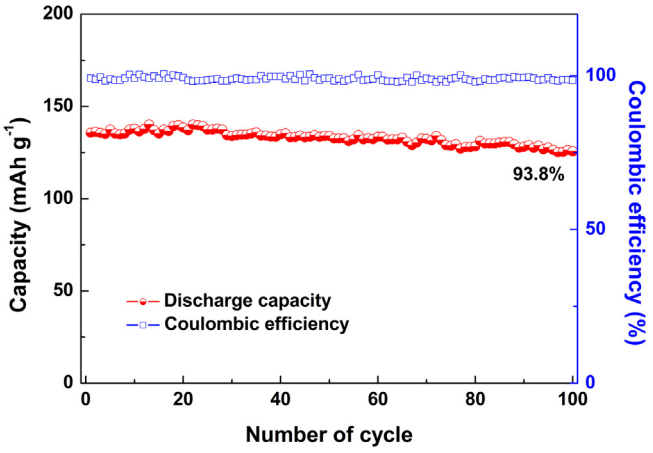

Fig. 6. The cycling performance and columbic efficiency of the core–shell composite cells cycled at a rate of 5 C in the voltage of 2.0–4.4 V at room temperature.

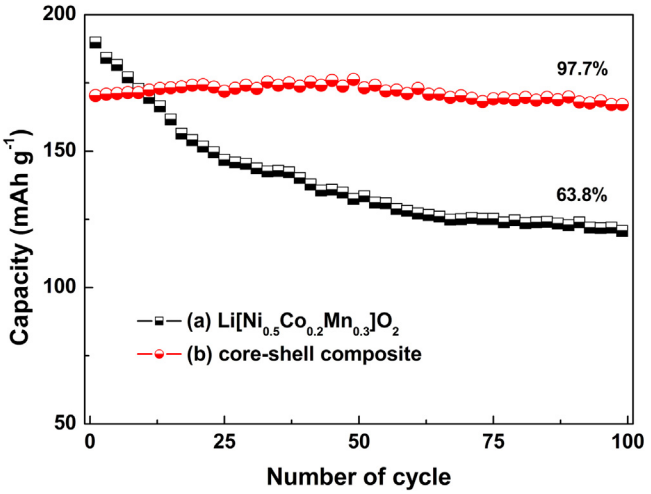

Fig. 7. Discharge capacity *versus* cycle number of (a) Li/core–shell composite and (b) Li/Li[$Ni_{0.5}Co_{0.2}Mn_{0.3}$]O_2 cells at a rate of 0.5 C in the voltage range of 2.0–4.4 V at 55 °C.

The electrochemical properties of the Li[$Ni_{0.5}Co_{0.2}Mn_{0.3}$]O_2–Li_2MnO_3 core–shell composite were compared with those of the pristine Li[$Ni_{0.5}Co_{0.2}Mn_{0.3}$]O_2 based on tests using the 2025 coin-type cell employing Li metal as the anode. The cells were cycled at a rate of 0.1 C (1 C corresponds to 200 mA g^{-1} current density) between 2.0 and 4.4 V at room temperature. Fig. 4 shows the first and second charge–discharge curves of the samples and the corresponding differential capacity profiles. As can be seen from Fig. 4a and b, two samples have one voltage region during the first two charge process cycled in the voltage range of 2.0–4.4 V. The voltage profiles started from the initial cell open circuit potential and monotonically increased to 4.4 V with a slope. The core–shell composite electrode delivered an initial discharge capacity of 180.4 mAh g^{-1}, which was slightly lower than that of the pristine Li[$Ni_{0.5}Co_{0.2}Mn_{0.3}$]O_2 (191.2 mAh g^{-1}) in the same voltage range. The Li_2MnO_3 is an electrochemical inert material when the voltage is less than 4.5 V, therefore the presence of the Li_2MnO_3 material as the outer shell reduced the total gravimetric capacity of the Li[$Ni_{0.5}Co_{0.2}Mn_{0.3}$]O_2–Li_2MnO_3 core–shell composite. To further examine the intercalation and deintercalation processes of lithium ions under different voltage limits, the capacities *versus* voltage plots were examined. The d*Q*/d*V* plots of the charge–discharge curves in Fig. 4a and b are shown in Fig. 4c and d, respectively. One pair of peaks at about 3.70–3.90 V was clearly seen in both initial and second cycles during the charge–discharge processes for both the electrodes, but the peak positions were slightly different. This pair of peaks was mainly attributed to the redox reactions of Ni^{2+}/Ni^{4+} and Co^{3+}/Co^{4+}, which correspond to the voltages region located at <4.5 V in Fig. 4a and b. The valence of manganese in the Li[$Ni_{0.5}Co_{0.2}Mn_{0.3}$]O_2 and Li_2MnO_3 compounds is +4, which is electrochemically inactive in the voltage range of 2.0–4.4 V. So the manganese doesn't take part in the charge–discharge reaction.

The variation of discharge capacity as a function of cycle number is given in Fig. 5. The cells were charged at a rate of 0.2 C and discharged at 0.5 C in the voltage range of 2.0–4.4 V at room temperature. The Li[$Ni_{0.5}Co_{0.2}Mn_{0.3}$]O_2 electrode delivered an initial discharge capacity of 177.4 mAh g^{-1}, and rapidly decreased to 131.8 mAh g^{-1} after 200 cycles with only 74.7% capacity retention. However, the core–shell composite electrode exhibited significantly improved cycling performance though delivering lower initial discharge capacity of 160.3 mAh g^{-1}. After 200 cycles, the Li/core–shell composite cells exhibited excellent capacity retention of 98.8%. Fig. 6 shows the electrochemical performance of the core–shell composite electrode cycled at a high rate of 5 C in the voltage range of 2.0–4.4 V at room temperature. The Li/core–shell composite cells can deliver a discharge capacity of 135.4 mAh g^{-1} with 93.8% capacity retention after 100 cycles. Particularly, the electrode exhibited an average value of coulombic efficiency more than 99.5%. The results indicate that the Li_2MnO_3 outer layer could effectively improve the cycling performance of the Li[$Ni_{0.5}Co_{0.2}Mn_{0.3}$]O_2. In order to further evaluate the high temperature stability of the samples, the cells were cycled at elevated temperature of 55 °C at a rate of 0.5 C in the voltage range of 2.0–4.4 V, as shown in Fig. 7. The capacity retention of the pristine Li[$Ni_{0.5}Co_{0.2}Mn_{0.3}$]O_2 was only 63.8% after 100 cycles, while the core–shell composite electrode showed superior cycling stability with capacity retention of 97.7% during the same cycling period. The improved cycle performance of the core–shell composite probably can be ascribed to the existence of the Li_2MnO_3 outer layer, which can effectively hinder the direct contact between the $LiNi_{0.5}Co_{0.2}Mn_{0.3}O_2$ core and electrolyte to stabilize the near-surface region of the active core material and reduce its reactivity with electrolyte. Consequently, the increase of interfacial impedance can be suppressed, and the long-term cycling stability can be maintained. From above experimental results, it is believed that the cycle instability of the nickel-rich Li[$Ni_{0.5}Co_{0.2}Mn_{0.3}$]O_2 was successfully overcome by the construction of core–shell architecture with a stable Li_2MnO_3 outer shell.

Cyclic voltammetry (CV) is a complementary and well-suited technique to evaluate the electrochemical performance of the electrode material [38,39]. The CV was conducted to understand the behavior of the as-prepared samples. Fig. 8 compares the cyclic voltammograms of pristine Li[$Ni_{0.5}Co_{0.2}Mn_{0.3}$]O_2 and core–shell composite obtained at a scan rate of 0.1 mV s^{-1} between 2.0 and 4.5 V at room temperature. Obviously, the anodic peak in first cycle

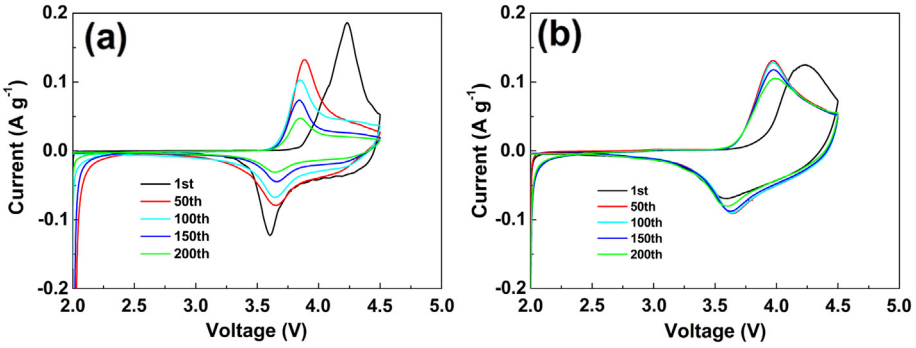

Fig. 8. Cyclic voltammograms of 1st, 50th, 100th, 150th and 200th cycles for (a) the pristine Li[$Ni_{0.5}Co_{0.2}Mn_{0.3}$]O_2 and (b) the core–shell composite between 2.0 and 4.5 V at a scan rate of 0.1 mV s^{-1} at room temperature.

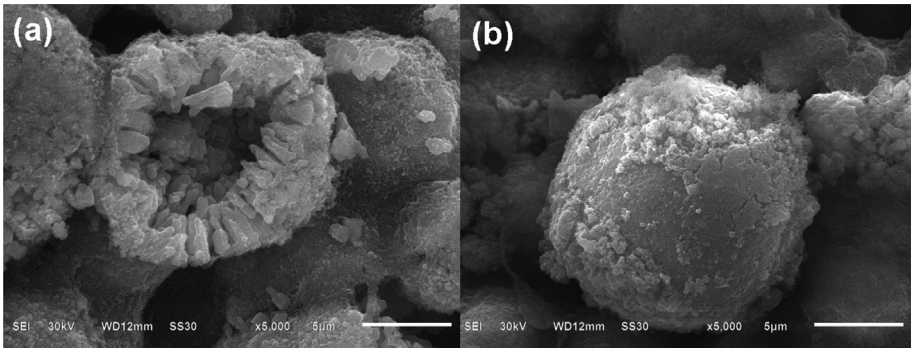

Fig. 9. SEM images of (a) $Li[Ni_{0.5}Co_{0.2}Mn_{0.3}]O_2$ and (b) core–shell composite particles after 200 cycles at a rate of 0.5 C in the voltage range of 2.0–4.4 V at room temperature.

occurred at ~4.22 V, whereas the main cathodic peak was located at ~3.60 V for both the samples. In the subsequent cycles, the anodic peak shifted to lower voltage of ~3.95 V, but the corresponding cathodic peak shifted only slightly, by ~0.05 V, to a higher voltage. The shift in the anodic peak voltage was an indication of the activation process of the electrode in the first cycle. In the case of the pristine $Li[Ni_{0.5}Co_{0.2}Mn_{0.3}]O_2$, as shown in Fig. 8a, the intensity of the redox peaks distinctly decreased during 1–200 cycles, which was indicative of large capacity-fading for the $Li[Ni_{0.5}Co_{0.2}Mn_{0.3}]O_2$ electrode. On the other hand, the CV curves of the core–shell composite displayed slightly decrease of the peak currents (Fig. 8b), suggesting that the cyclability of the core–shell composite was better than that of the pristine one. This shows that the Li_2MnO_3 outer shell could impede the electrolyte decomposition on the surface of the $Li[Ni_{0.5}Co_{0.2}Mn_{0.3}]O_2$ particle or suppress the phase transformation of the cathode material. As a result, the cycling performance of the core–shell composite was improved significantly.

To investigate the influence of the Li_2MnO_3 outer shell on the morphologies of the core–shell composite, SEM images of the cycled electrodes were recorded. Fig. 9 compares the morphologies of the $Li[Ni_{0.5}Co_{0.2}Mn_{0.3}]O_2$ and the core–shell composite electrodes after 200 cycles. As illustrated in Fig. 9a, the spherical $Li[Ni_{0.5}Co_{0.2}Mn_{0.3}]O_2$ particle appeared serious damage and formed a hollow sphere morphology. During the long-term cycling, the surface of $Li[Ni_{0.5}Co_{0.2}Mn_{0.3}]O_2$ particles were completely exposed, which could be subjected to continuous HF attack from the electrolyte. In addition, the oxygen was removed from the highly delithiated $Li_{1-\delta}[Ni_{0.5}Co_{0.2}Mn_{0.3}]O_2$ host structure, resulting in many oxygen vacancies. These could well explain the reasons of the hollow structure of the $Li[Ni_{0.5}Co_{0.2}Mn_{0.3}]O_2$ particle after cycling. On the contrary, the core–shell composite particle exhibited almost intact sphere morphology even after long-term cycling. Although the attack of the electrolyte to the surface of the core–shell composite particles may not be excluded, the eventual damaged parts do not affect the delivery capacity since the thick Li_2MnO_3 shell is electrochemically inactive under the upper cut-off voltage of 4.5 V. All the above discussed experimental evidences concur to demonstrate that the core–shell composite with a stable Li_2MnO_3 shell is a winning strategy for protecting the layered nickel-rich $Li[Ni_{0.5}Co_{0.2}Mn_{0.3}]O_2$ material, conferring to it a very high stability and a superior electrochemical performance.

Fig. 10 shows differential scanning calorimetry (DSC) curves of the $Li[Ni_{0.5}Co_{0.2}Mn_{0.3}]O_2$ and core–shell composite in the charged state to 4.4 V. The pristine $Li[Ni_{0.5}Co_{0.2}Mn_{0.3}]O_2$ electrode had a large exothermic peak at ~274.8 °C with an onset of decomposition near 250.0 °C, and the reaction released heat of 1296.5 J g^{-1}. However, the core–shell composite showed that the reaction took place at a higher temperature of 285.6 °C with a low heat generation of 594.3 J g^{-1}. These results clearly show that the core–shell composite has batter thermal stability than the pristine one. The improved thermal stability of the core–shell composite is probably due to the thermally stable Li_2MnO_3 outer shell, which can prevent the highly delithiated $Li_{1-\delta}[Ni_{0.5}Co_{0.2}Mn_{0.3}]O_2$ from being reduced, which, in turn, can suppress the oxygen release from the host structure.

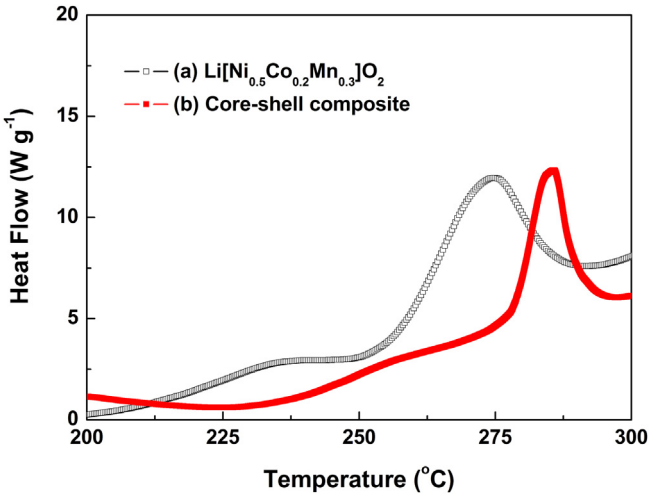

Fig. 10. DSC traces of the $Li/Li[Ni_{0.5}Co_{0.2}Mn_{0.3}]O_2$ and Li/core–shell composite cells.

4. Conclusions

The novel spherical core–shell composite, in which the nickel-rich $Li[Ni_{0.5}Co_{0.2}Mn_{0.3}]O_2$ as the core and Li_2MnO_3 as the outer shell, was successfully synthesized. The thickness of the outer shell was about 0.3 μm, which was not easy to fall off during the long-term cycling. The core–shell composite delivered a high capacity of 180.4 mAh g^{-1} at a rate of 0.1 C in the voltage range of 2.0–4.4 V. Most importantly, the core–shell material showed excellent cycling performance with capacity retention of 98.8% at a rate of 0.5 C, and 93.8% capacity retention at a high rate of 5 C at room temperature. When cycled at elevated 55 °C, the as-prepared sample still exhibited only 2.3% capacity loss after 100 cycles. The improved thermal stability of the core–shell composite was also successfully obtained due to a stable Li_2MnO_3 shell. The core–shell morphological strategy here, in which the nickel-rich $Li[Ni_{0.5}Co_{0.2}Mn_{0.3}]O_2$ as the core to deliver high capacity and the stable Li_2MnO_3 as the shell to obtain excellent stability, has shown a marked merit for improving the performance of $Li[Ni_{0.5}Co_{0.2}Mn_{0.3}]O_2$, especially at high voltages and high temperatures, and this technology can be

extended to the synthesis of other new high-performance cathode materials for the application of lithium ion batteries.

Acknowledgments

This work was funded by the National Natural Science Foundation of China under project No. 20871101, Scientific Research Fund of Hunan Provincial Education Department No. 09c947, Key Project of Science and Technology Department of Human Province Government under project No. 2009WK2007, Colleges and Universities in Hunan Province plans to graduate research and innovation under project No. CX2012Bb57.

References

[1] B. Zhao, X. Yu, R. Cai, R. Ran, H. Wang, Z. Shao, J. Mater. Chem. 22 (2012) 2900–2907.
[2] Y. Zhou, J. Wang, Y. Hu, R. O'Hayre, Z. Shao, Chem. Commun. 46 (2010) 7151–7153.
[3] Eun-Sung Lee, Ashfia Huq, Hong-Young Chang, Arumugam Manthiram, Chem. Mater. 24 (2012) 600–612.
[4] A.M. Cao, J.S. Hu, H.P. Liang, L.J. Wan, Angew. Chem. Int. Ed. 44 (2005) 4391–4395.
[5] C.R. Fell, D.H. Lee, Y.S. Meng, J.M. Gallardo-Amores, E. Moran, M.E. Arroyo-de Dompablo, Energy Environ. Sci. 5 (2012) 6214–6224.
[6] A. Manthiram, J. Phys. Chem. Lett. 2 (2011) 176–184.
[7] B. Dunn, H. Kamath, J.M. Tarascon, Science 334 (2011) 928–935.
[8] C. Liu, F. Li, L.P. Ma, H.M. Cheng, Adv. Mater. 22 (2010) E28–E62.
[9] Yang-Kook Sun, Zonghai Chen, Hyung-Joo Noh, Dong-Ju Lee, Hun-Gi Jung, Yang Ren, Steve Wang, Chong Seung Yoon, Seung-Taek Myung, Khalil Amine, Nat. Mater. 11 (2012) 942–947.
[10] Yang-Kook Sun, Bo-Ram Lee, Hyung-Ju Noh, Huiming Wu, Seung-Taek Myung, Khalil Amine, J. Mater. Chem. 21 (2011) 10108–10112.
[11] Yang-Kook Sun, Seung-Taek Myung, Myung-Hoon Kim, Jai Prakash, Khalil Amine, J. Am. Chem. Soc. 127 (2005) 13411–13418.
[12] R.B. Wright, J.P. Christophersen, C.G. Motloch, J.R. Belt, C.D. Ho, V.S. Battaglia, J.A. Barnes, T.Q. Duong, R.A. Sutula, J. Power Sources 112 (2003) 865–869.
[13] Kai Yang, Li-Zhen Fan, Jia Guo, Xuanhui Qu, Electrochim. Acta 63 (2012) 363–368.
[14] Wen Liu, Miao Wang, Xing long Gao, Weidong Zhang, Jitao Chen, Henghui Zhou, J. Alloys Compd. 543 (2012) 181–188.
[15] Yansong Bai, Xianyou Wang, Shunyi Yang, Xiaoyan Zhang, Xiukang Yang, Hongbo Shu, Qiang Wu, J. Alloys Compd. 541 (2012) 125–131.
[16] Yang-Kook Sun, Dong-Hui Kim, Chong Seung Yoon, Seung-Taek Myung, Jai Prakash, Khalil Amine, Adv. Funct. Mater. 20 (2010) 485–491.
[17] J.S. Kim, C.S. Johnson, J.T. Vaughey, M.M. Thackeray, S.A. Hackney, W. Yoon, C.P. Grey, Chem. Mater. 16 (2004) 1996–2006.
[18] M.M. Thackeray, C.S. Johnson, J.T. Vaughey, N. Li, S.A. Hackney, J. Mater. Chem. 15 (2005) 2257–2267.
[19] Z. Lu, D.D. MacNeil, J.R. Dahn, Electrochem. Solid-State Lett. 4 (2001) A191–A194.
[20] Z. Lu, L.Y. Beaulieu, R.A. Donaberger, C.L. Thomas, J.R. Dahn, J. Electrochem. Soc. 149 (2002) A778–A785.
[21] J. Breger, Y.S. Meng, Y. Hinuma, S. Kumar, K. Kang, Chem. Mater. 18 (2006) 4768–4781.
[22] A.R. Armstrong, M. Holzapfel, P. Novak, C.S. Johnson, S.H. Kang, M.M. Thackeray, P.G. Bruce, J. Am. Chem. Soc. 128 (2006) 8694–8698.
[23] J. Gao, J. Kim, A. Manthiram, Electrochem. Commun. 11 (2009) 84–86.
[24] Jin-Long Liu, Jie Wang, Yong-Yao Xia, Electrochim. Acta 56 (2011) 7392–7396.
[25] J.M. Zheng, X.B. Wu, Y. Yang, Electrochim. Acta 56 (2011) 3071–3078.
[26] M.M. Thackeray, S.H. Kang, C.S. Johnson, J.T. Vaughey, R. Benedek, S.A. Hackney, J. Mater. Chem. 17 (2007) 3112–3125.
[27] M.-H. Lee, Y.-J. Kang, S.-T. Myung, Y.-K. Sun, Electrochim. Acta 50 (2004) 939–948.
[28] K.K. Cheralathan, Na Young Kang, Hun Su Park, You Jin Lee, Won Choon Choi, Young Soo Ko, Yong-Ki Park, J. Power Sources 195 (2010) 1486–1494.
[29] Shunyi Yang, Xianyou Wang, Xiukang Yang, Ziling Liu, Yansong Bai, Yingping Wang, Hongbo Shu, J. Solid State Electrochem. 16 (2012) 2823–2836.
[30] Xiukang Yang, Xianyou Wang, Qiliang Wei, Hongbo Shu, Li Liu, Shunyi Yang, Benan Hu, Yunfeng Song, Guishan Zou, Liang Hu, Lanhua Yi, J. Mater. Chem. 22 (2012) 19666–19672.
[31] Jiangang Li, Li Wang, Qian Zhang, Xiangming He, J. Power Sources 189 (2009) 28–33.
[32] H. Deng, I. Belharouak, H. Wu, D. Dambournet, K. Amine, J. Electrochem. Soc. 157 (2010) A776–A781.
[33] A. Boulineau, L. Croguennec, C. Delmas, F. Weill, Solid State Ionics 180 (2010) 1652–1659.
[34] K. Karthikeyan, S. Amaresh, G.W. Lee, V. Aravindan, H. Kim, K.S. Kang, W.S. Kim, Y.S. Lee, Electrochim. Acta 68 (2012) 246–253.
[35] Sang-Ho Park, Yuichi Sato, Jae-KooK Kim, Yun-Sung Lee, Mater. Chem. Phys. 102 (2007) 225–230.
[36] M.M. Thackeray, S.-H. Kang, C.S. Johnson, J.T. Vaughey, S.A. Hackney, Electrochem. Commun. 8 (2006) 1531–1538.
[37] S.H. Park, S.H. Kang, I. Belharouak, Y.K. Sun, K. Amine, J. Power Sources 177 (2008) 177–183.
[38] K.M. Shaju, G.V. Subba Rao, B.V.R. Chowdari, Electrochim. Acta 48 (2003) 1505–1514.
[39] J.P. Cho, H.S. Jung, Y.C. Park, G.B. Kim, H.S. Lim, J. Electrochem. Soc. 147 (2000) 15–20.